Efficient one-third harmonic generation in highly Germania-doped fibers enhanced by pump attenuation

Tianye Huang,[1, 2] Xuguang Shao,[2, *] Zhifang Wu,[1, 2] Timothy Lee,[3] Yunxu Sun,[2] Huy Quoc Lam,[2] Jing Zhang,[4] Gilberto Brambilla,[3] and Shum Ping[1, 2]

[1]CINTRA CNRS/NTU/THALES, UMI 3288, Research Techno Plaza, 50 Nanyang Drive, Level 6, Singapore
[2]School of Electrical and Electronics Engineering, Nanyang Technological University, Singapore
[3]Optoelectronics Research Center, University of Southampton, Southampton, SO17 1BJ, UK
*[4]National Metrology Centre, Agency for Science, Technology and Research (A*STAR), 118221 Singapore*

We provide a comprehensive study on one-third harmonic generation (OTHG) in highly Germania-doped fiber (HGDF) by analyzing the phase matching conditions for the step index-profile and optimizing the design parameters. For stimulated OTHG in HGDF, the process can be enhanced by fiber attenuation at the pump wavelength which dynamically compensates the accumulated phase-mismatch along the fiber. With 500 W pump and 35 W seed power, simulation results show that a 31% conversion efficiency, which is 4 times higher than the lossless OTHG process, can be achieved in 34 m of HGDF with 90 mol. % GeO_2 doping in the core.

1. Introduction

Although third harmonic generation (THG) has been intensively investigated both theoretically and experimentally in past literature [1–4], the inverse process of one-third harmonic generation (OTHG) remains a new topic that has been attracting increasing research attentions. Previous studies on OTHG categorize the process into two kinds, namely, spontaneous downconversion and stimulated downconversion. The former was recently analyzed by Gravier [5], Corona [6] and Richard [7]. Inherently, however, the conversion efficiency is extremely low. Stimulated downconversion, on the other hand, is more appealing as the OTHG process can be seeded to achieve high conversion efficiency. In [8], Afshar et al. report a method for evaluating the maximum conversion efficiency of lossless THG and OTHG process, in which the maximum conversion efficiency is determined by waveguide structure and total input power. However, in real experiments, attenuation always exists and affects the total power along the interaction medium. Furthermore, because of the triple relationship of wavelength between pump and signal in OTHG, the loss profile at the two wavelengths can be quite different, which should consequently be taken into consideration along with the waveguide structure and power level when evaluating the performance of OTHG. High conversion efficiency can be expected by optimizing these parameters.

Highly Germania-doped fiber (HGDF) consisting of a Germania-Silica core within a Silica cladding has attracted extensive interest in the past years [9–13]. Also, HGDF is a good candidate for OTHG because of its capability to achieve inter-modal phase matching and low attenuation characteristics around 0.5 μm and 1.5 μm. However, to date, the role of doping concentration in HGDFs for OTHG has yet to be addressed in detail.

In this paper, a comprehensive study of the stimulated OTHG process in HGDFs is performed. The phase matching parameters in step-index fiber are designed. Different modes are discussed in terms of overlap integrals and the most suitable one is then chosen for inter-modal phase matching. The performances of different HGDFs are simulated and evaluated along with the possibility for pump attenuation in playing a contributing role towards efficient OTHG.

2. Phase matching in HGDFs

OTHG and THG share the same phase matching conditions, which have previously been discussed for glass microfibers [1, 2]. The main disadvantage is that the interactive length is limited to several centimeters because of the difficulty in fabricating long microfibers whilst maintaining the small diameter required for phase matching. High-delta micro-structured fibers were also employed to realize phase matching [14]. More recently, Tarnowski et al. proposed an approach to compensate for the phase mismatch for THG by using quasi-phase matching technique based on the grating written in the fiber [15]. However, the fabrication processes of these fibers are quite complicated. On the other hand, high numerical aperture (NA) fibers offer an attractive choice to achieve phase matching because the big fibers can be straightforwardly fabricated to much longer interactive lengths [6, 16]. Here we demonstrate a detailed analysis for phase matching conditions in HGDFs.

In the process of OTHG in optical fibers supporting several modes, a pump photon, oscillating at the circular frequency ω_3 with wave vector k_3, splits into a set of three photons with circular frequencies $\omega_1 = \omega_3/3$ and wave vector $k_1 = k_3/3$. This condition is equivalent to: $n_{\text{eff}}(\omega) = n_{\text{eff}}(3\omega)$, where n_{eff} is the effective index of the relevant mode. Here, we consider the phase matching between $\lambda_3 = 0.532$ μm (the pump wavelength) and $\lambda_1 = 1.596$ μm (the one-third harmonic wavelength). Figure 1 shows the material dispersion of pure and 10 mol. % GeO_2 doped silica. The Sellmeier functions for material dispersion are obtained from [17]. Due to uneven material dispersion curves, the cladding index at the pump wavelength exceeds the core index at the one-third harmonic wavelength. Hence, there is no overlap region between the effective index ranges for the two wavelengths in a step-index fiber with a core doping concentration of 10 mol. % and so phase matching between guided modes is impossible in such a weakly guiding fiber. In this case, guided modes at 1.596 μm can only match to the radiation modes at 0.532 μm, which suffer from large loss and small overlap integrals. The solution is to further increase the doping concentration to achieve a higher NA so that the effective index areas at the two wavelengths can overlap leading to the possibility of phase matching between two guided modes.

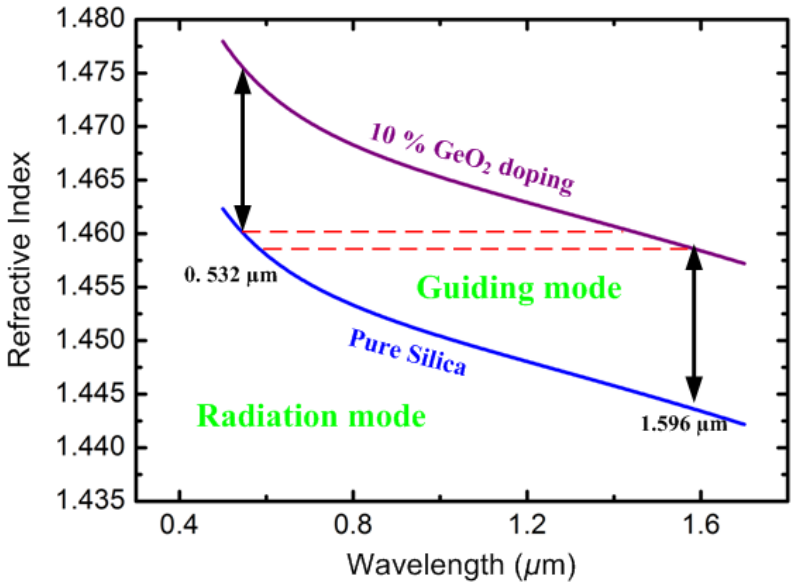

Fig. 1. Material dispersion of pure silica (cladding) and 10 mol. % GeO_2 doped silica (core). The arrows mark the range in which the effective indices of guided modes at λ = 0.532 μm and 1.596 μm reside.

By solving the rigorous modal eigenvalue equations for a step index profile in HGDF [18], Fig. 2 demonstrates the effective indices of the modes at two wavelengths as a function of core diameter with a higher 30 mol. % doping concentration in the fiber core. Only hybrid HE and EH modes are considered since the overlap with transverse TE and TM modes is zero. Obviously, with sufficient doping concentration, a large number of high-order modes at 0.532 μm can find a core diameter for phase matching the mode HE_{11} at 1.596 μm. Because high-order modes are more difficult excite and have a smaller overlap with the fundamental mode, we restrict our discussion to the lower-order modes (EH_{31}, EH_{12}, HE_{32}, and HE_{13}).

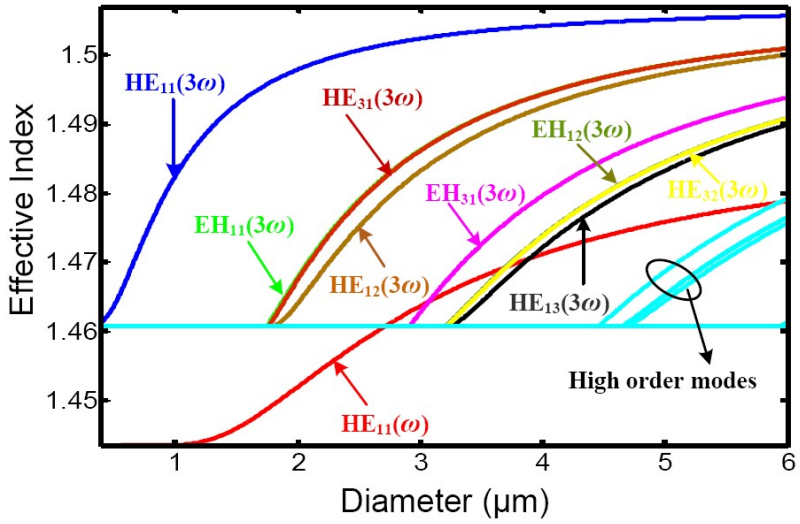

Fig. 2. Effective indices of different modes as a function of core diameter with a Germania core doping concentration of 30 mol. %.

To assess which of the possible phase match points would be most efficient for OTHG, the modal overlaps J_3 between the $HE_{11}(\omega)$ and each higher order ω_3 mode were calculated according [1]:

$$J_3 = \iint_{A_{NL}} (F_1^* \cdot F_3)(F_1^* \cdot F_1^*) dS \qquad (1)$$

where F_1 and F_3 denote the power-normalized electric field distributions of the HE_{11} mode at 1.596 μm and the phase matched higher order mode at 0.532 μm, respectively. The characteristics of the four phase-matched modes mentioned above as a function of doping concentration are demonstrated in Fig. 3. It can be seen from Fig. 3(a) that their effective indices increase with doping concentration because of the higher refractive index of GeO_2. In Fig. 3(b), the phase matching diameters decrease with increased doping since the modes are more tightly confined within the core region. Although the diameter for phase matching with mode the HE_{13} mode is larger than the others, this mode has the largest overlap integrals J_3, and is therefore the most promising choice for ensuring an efficient OTHG process. This finding is valid because both HE_{11} and HE_{13} are circularly symmetric and have their largest field intensity in the centre. Note that the overlap increases with increasing doping concentration as shown in Fig. 3(c), again due to the increase in modal confinement.

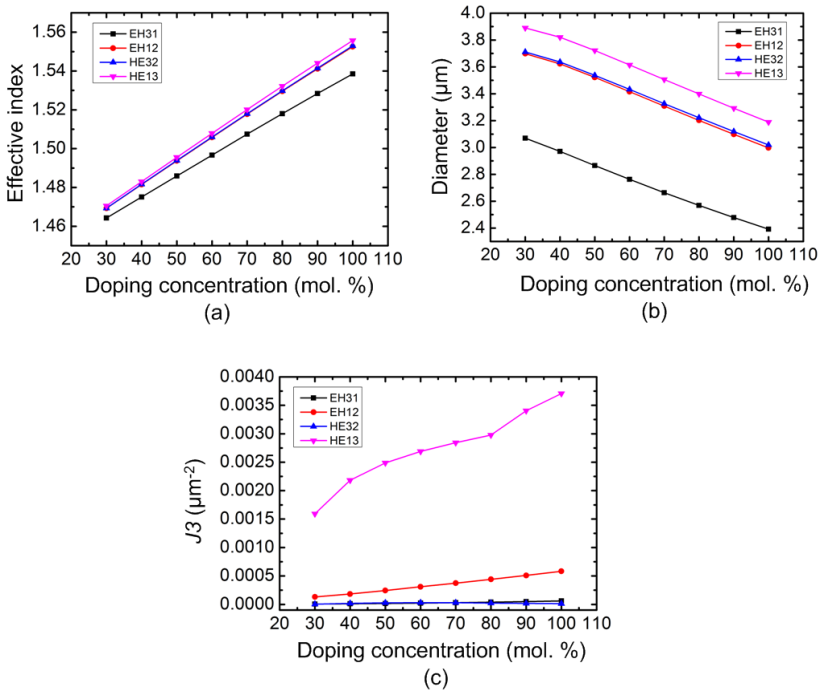

Fig. 3. (a) Effective index, (b) core diameter and (c) J_3 as a function of doping concentration for modes at 4 different phase matched points.

3. Analysis and simulation results

Assuming the fields at ω_1 and $3\omega_1$ are in different but single propagating modes of the fiber, the fields can be described by slowly varying amplitudes $A_i(z)$, where $i = 1$ refers to the one-third harmonic, and $i = 3$ refers to the pump. The following set of equations can then be derived [1]:

$$\frac{\partial A_1}{\partial z} = -\frac{\alpha_1}{2} A_1 + i\gamma_0[(J_1 \mid A_1 \mid^2 + 2J_2 \mid A_3 \mid^2)A_1 + J_3 (A_1^*)^2 A_3 e^{i\Delta\beta z}] \tag{2}$$

$$\frac{\partial A_3}{\partial z} = -\frac{\alpha_3}{2} A_3 + i\gamma_0[(6J_2 \mid A_1 \mid^2 + 3J_5 \mid A_3 \mid^2)A_3 + J_3^* A_1^3 e^{-i\Delta\beta z}] \tag{3}$$

where J_1, J_2, J_3, and J_5 denote the modal overlap integrals for one-third harmonic self-phase modulation (SPM), pump harmonic cross-phase modulation (XPM), pump harmonic conversion, and pump SPM, α_i is the loss coefficient, $\Delta\beta = \beta(3\omega) - 3\beta(\omega)$ is the propagation constant mismatch, and $\gamma_0 = 2\pi n^{(2)}/\lambda$, where $n^{(2)}$ is the nonlinear refractive index coefficient. For GeO_2-doped silica, a linear relation with silica of $n^{(2)} = (0.0552Conc + 2.44) \times 10^{-20}$ m^2/W is used to estimate nonlinear refractive index, where *Conc* is the mole concentration [19]. The power of each mode is given by $|A_i|^2$. Defining $A_1 = \sqrt{P_1} e^{i\varphi_1}$, $A_3 = \sqrt{P_3} e^{i\varphi_3}$, and $\psi = \Delta\beta z + \varphi_3 - 3\varphi_1$, the coupled mode equations can be rewritten as:

$$\frac{dP_1}{dz} = -\alpha_1 P_1 - 2J_3\gamma_0 P_1^{\frac{3}{2}} P_3^{\frac{1}{2}} \sin\psi \tag{4}$$

$$\frac{dP_3}{dz} = -\alpha_3 P_3 + 2J_3\gamma_0 P_1^{\frac{3}{2}} P_3^{\frac{1}{2}} \sin\psi \tag{5}$$

$$\frac{d\psi}{dz} = \Delta\beta + \gamma_0[(6J_2 - 3J_1)P_1 + (3J_5 - 6J_2)P_3 + J_3(P_1^{\frac{3}{2}}P_3^{-\frac{1}{2}} - 3P_1^{\frac{1}{2}}P_3^{\frac{1}{2}})\cos\psi] \quad (6)$$

As shown in Eqs. (4) and (5), the power flow direction is determined by the sign of *sin* ψ, if *sin* $\psi > 0$, it is THG process, otherwise OTHG. If *sin* $\psi < 0$ is satisfied at the input of the interactive media and the right hand side of Eq. (6) is kept approximately to be 0, power can be transferred from the pump (P_3) to signal (P_1) continuously. However, as P_1 increases and P_3 decreases, Eq. (6) becomes none zero and ψ deviates from *sin* $\psi < 0$ because of the fiber loss and different Kerr coefficients ($6J_2$-$3J_1$ and $3J_5$-$6J_2$), hence changing the varying rate and direction of the power flow. Additionally, according to Eq. (4), it is easy to note that the varying rate of P_1 can be quite low with a small seed light (P_1) at the input of the interactive media because the varying rate is proportional to $P_1^{1.5}$. With small P_1, simply increasing the pump power contributes little to the conversion rate improvement. This feature is totally different with THG, whose power changing rate can be increased by strong pump, as shown in Eq. (5). Therefore, in order to obtain efficient OTHG, a potential method is to stimulate the process with powerful seed. The theoretical analysis for lossless OTHG proposed in [8] points out that the maximum conversion efficiency is dominated by the total input power and waveguide structure. In the above mentioned HGDF, according to our calculation, the relationship of overlap integrals cannot fulfill the special requirements mentioned in [8] for efficient OTHG process. However, because of the existence of loss which can be quite different at pump and signal wavelengths, the conversion mechanics are slightly different. Since the losses of pure silica and GeO_2 at 0.532 μm are about 11 dB/km and 300 dB/km and 0.2 dB/km and 0.6 dB/km at 1.596 μm [20], we use a linear relation to approximate the HGDF loss at different doping concentration, the attenuation coefficient at longer wavelength is much smaller which raises the possibility for dynamically compensating for the phase mismatch during propagation along fiber.

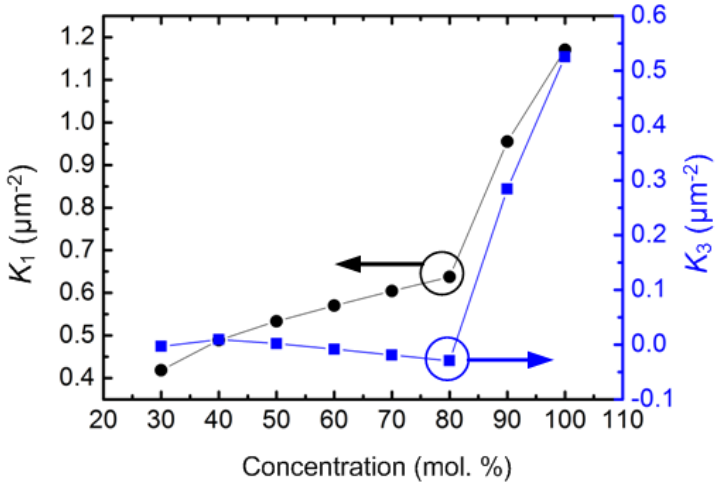

Fig. 4. K_1 and K_3 as a function of doping concentration

In order to investigate the parametric process in the above mentioned HGDF, we return to Eq. (6) which shows that ψ is determined by four terms including a linear $\Delta\beta$ term (regarded as constant along a longitudinally invariant fiber). We also define the Kerr coefficients $K_1 = 6J_2$-$3J_1$, and $K_3 = 3J_5$-$6J_2$, whose values as a function of doping concentration are demonstrated in Fig. 4. Their behavior can be divided into three regimes:

(1) 0 < J_3 << K_3 < K_1 (90 mol. % and 100 mol. % doping)

Since K_1 and K_3 are much larger than J_3, the last term of Eq. (6) can be neglected and the equation approximated as:

$$\frac{d\psi}{dz} = \Delta\beta + \gamma_0(K_1P_1 + K_3P_3) \tag{7}$$

In this case, if sin $\psi < 0$ is fulfilled at the input of the fiber, power can transfer from P_3 to P_1 due to OTHG process. Given this is a lossless process, the increasing rate of K_1P_1 must be faster than the decreasing rate of K_3P_3 because $K_1 > K_3$, and therefore after propagating along a short distance of fiber, the power will transfer from P_1 to P_3 again then oscillating between the two waves. However, the condition will be different considering large pump loss. Combining the effect of power attenuation caused by parametric processes (i.e. the transfer of power to the other wavelength) and fiber loss, the increment of K_1P_1 can be comparable with the decrement of K_3P_3 so that ψ changes slowly and P_1 can build up continuously over a long fiber length. When ψ changes to make sin $\psi > 0$, the THG process starts and power begins to transfer from P_1 to P_3, reducing K_1P_1 and increasing K_3P_3. Similarly, the changing rate of K_1P_1 is faster than K_3P_3, meanwhile a large α_3 prevents the increasing of K_3P_3. These two terms cannot balance with each other, and therefore ψ changes fast and it is difficult to maintain sin $\psi > 0$. ψ will vary such that sin ψ falls below 0 after a short propagation length and return to OTHG process again, as a result P_1 can accumulate. In this case, OTHG can benefit from the large loss at pump wavelength.

(2) 0 < J_3 ≈ K_3 << K_1 (40 mol. % and 50 mol. % doping)

This case is similar to the first one, but the balance between phase terms is more difficult because of the small values of K_3 and J_3. If the pump loss is too small, the K_1P_1 term will dominate the phase varying rate and make the process close to the lossless one. Even if, the loss is large enough to compensate phase changing at the input of fiber, OTHG cannot benefit from pump attenuation for long distances since the pump power decays exponentially along the fiber. After a certain distance, the balance can be break.

(3) $K_3 < 0 < J_3 << K_1$ (30 mol. %, 60 mol. %, 70 mol. % and 80 mol. % doping)

In the OTHG process, both K_1P_1 and K_3P_3 increase while the changing direction of the J_3 term (the last term in Eq. (6)) is determined by the sign of cos ψ which can be positive or negative during OTHG process. Nevertheless, J_3 is too small compared with K_1, so K_1P_1 and K_3P_3 lead to a fast phase variation. While the OTHG buildup region is restricted to $-\pi < \psi < 0$, ψ cannot stay in this favorable region for a long propagating length. Therefore, it is difficult to realize efficient OTHG.

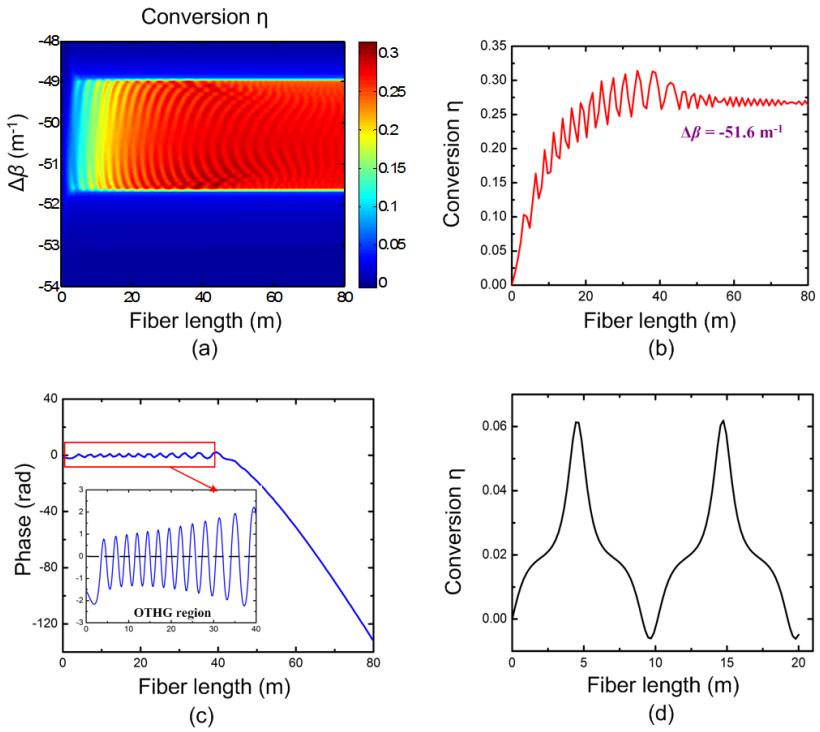

Fig. 5. (a) Contour map of conversion efficiency in lossy 90 mol. % HGDF with different $\Delta\beta$, (b) conversion efficiency variation along fiber length with $\Delta\beta = -51.6$ m^{-1}, (c) phase variation along fiber and (d) efficiency performance without loss

To verify our analysis mentioned above, we used the Runge-Kutta method in MATLAB to numerically calculate Eqs. (2) and (3) to investigate the designed fiber with different doping concentrations. The pump and signal powers are set to be 500 W, and 35 W, respectively and initial phase difference $\psi(0) = -\pi/2$. For a lossy interaction, the conversion efficiency is given by $\eta = (P_{1out} - P_1(0))/P_3(0)$, where P_{1out} is the power of the one-third harmonic at the output. In Fig. 5(a), we give the efficiency contour map with a 90 mol. % doping concentration with different $\Delta\beta$ values which make the right hand side of Eq. (5) approximately zero. In this case, an OTHG conversion efficiency of more than 30% can be achieved in a propagation constant mismatch range from -51 m^{-1} to -51.6 m^{-1} by taking advantage of the better balance between power transfer and power attenuation. It can be seen from Fig. 5(b) that within 34 m of fiber, the transfer of power from the pump to the seed (i.e. $-\pi < \psi < 0$) can continue over a net OTHG interaction length longer than that of THG. Although the system oscillates between OTHG and THG during propagation, during the latter process the phase change rate is much faster, and hence the phase quickly returns to the range required for OTHG. Consequently, the one-third harmonic experiences an overall growth, especially at the beginning of the fiber where the strong power decay of P_3 compensates the faster phase changing term K_1P_1. The OTHG power oscillates up until the pump depletes. Figure 5(c) illustrates the phase evolution along the fiber by solving Eq. (5), as predicted, K_1P_1 and K_3P_3 dominate the phase variation and balance with each other within 34 m fiber length. The total phase is more confined in the region favoring OTHG ($-\pi$, 0) as shown in the zoomed-in inset. After this length, the phase starts to change fast because the pump depletes and the nonlinear phase shift caused by the smaller P_1 is not sufficient to compensate $\Delta\beta$. In comparison, for lossless OTHG, the maximum conversion efficiency we can obtain is about 6% as shown in Fig. 5(d), which is 4 times smaller than the loss assisted process. Note that high conversion is not limited by the specific input power condition used here. For a 500 W pump, which can be easily achieved by frequency doubling

from an Nd: YAG laser, 35 W is close to the minimum power needed for a high conversion (higher than 30%). To further investigate the efficiency with different input condition, Fig. 6(a) presents the maximum achievable efficiency and corresponding fiber length with 90 mol. % doping with respect to the seed power, when the pump power is fixed to be 500 W. Clearly, we can conclude that higher seed power leads to higher conversion efficiency and reduces the required fiber length. On the other hand, if the seed power is fixed at 35 W, the proposed scheme can also remain efficient when the input pump power varies in a large range as shown in Fig. 6(b). According to the main trends of the two curves, increasing the pump power will reduce the maximum conversion and increase the required fiber length. This is reasonable because a larger pump power speeds up the phase variation and contributes less to the power transferring rate comparing with seed power. However, since $0 < J_3 << K_3 < K_1$, the OTHG process is still overall enhanced over the fiber link. Therefore, in the specially-designed HGDF, efficient OTHG can be realized within a large power range of input pump and seed. Typically, they are not limited to the fixed 500 W pump and 35 W seed.

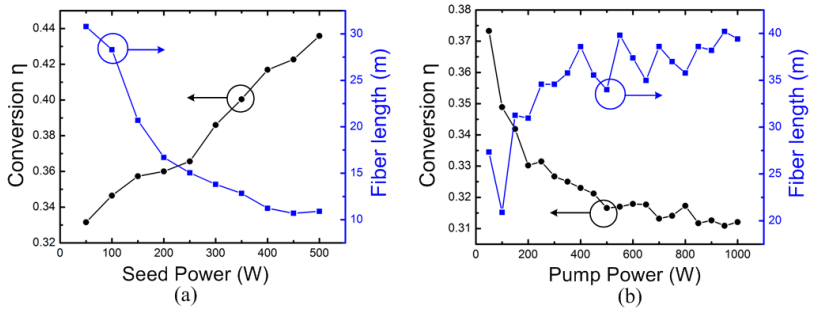

Fig. 6. Maximum conversion and corresponding fiber length with respect to (a) seed power when pump power is fixed at 500 W and (b) pump power when seed power is fixed at 35 W in 90 mol. % doping HGDF.

It should be noted that with high power input, Brillouin and Raman scattering process may act as additional attenuation mechanisms and affect the conversion efficiency. However, because there is no cavity or seed power at Brillouin and Raman scattering wavelengths in the proposed scheme, the power generated from these two nonlinear processes cannot be resonantly enhanced and must start from spontaneous processes with low efficiency. As the HGDF is designed to phase-match the pump and one-third harmonic wavelengths, with proper seed power, stimulated OTHG can happen immediately at the input of the fiber. Combining parametric attenuation and fiber loss, the pump power will deplete quickly and make other scattering processes more difficult to be efficient. Also, as shown in Fig. 6(b), a high efficiency is still expected even with lower pump powers and shorter fibers. For example, if the pump power is reduced to 100 W, nearly 35% conversion can still be achieved with 21 m of HGDF.

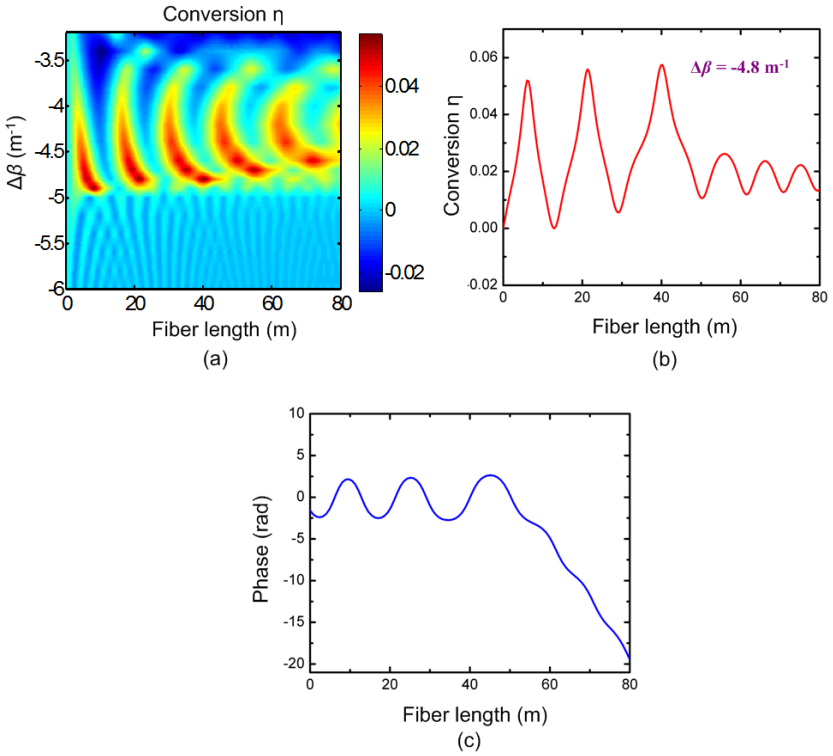

Fig. 7. (a) Contour map of conversion efficiency in 40 mol. % HGDF with different $\Delta\beta$, (b) conversion efficiency variation along fiber length with $\Delta\beta = -4.8$ m^{-1}, and (c) phase variation along fiber.

For the case of a weaker 40 mol. % doping concentration, Fig. 7(a) shows a contour map of OTHG conversion efficiency long fiber length with different propagation phase mismatch $\Delta\beta$. Relatively strong OTHG happens in the region -5 m^{-1} $< \Delta\beta < -4$ m^{-1}, however, maximum conversion efficiency is less than 6%. Note that the regions of negative η at $\Delta\beta > -3.5$ m^{-1} correspond to regimes in which the power is being transferred away from the seed to the pump wavelength. Figure 7(b) demonstrates the efficiency evolution with optimized $\Delta\beta = -4.8$ m^{-1}. According to our analysis above, η starts to build up at the input of the fiber reinforced by pump loss. Unfortunately, η can no longer continue increasing after passing through the third peak because P_3, which decays exponentially along the fiber, cannot balance the huge phase changing caused by K_1P_1 which limits the buildup of η. The phase variation given in Fig. 7(c) shows the net interactive fiber length for OTHG and THG is nearly the same, causing the one-third harmonic power difficult to be accumulated. This can also be explained by the huge difference of J_3, K_3, and K_1. Power attenuation of P_3 caused by both fiber and parametric attenuation are not enough to slow down the phase variation.

As we mentioned above, with doping concentrations of 30 mol. %, 60 mol. %, 70 mol. % and 80 mol. %, pump loss is no longer favorable for OTHG. The performances of these four doping concentration are demonstrated in Figs. 8(a)–8(d), respectively. From the efficiency contour maps, it is apparent that η cannot go up higher after reaching their first efficiency peak which limits conversion to < 5%.

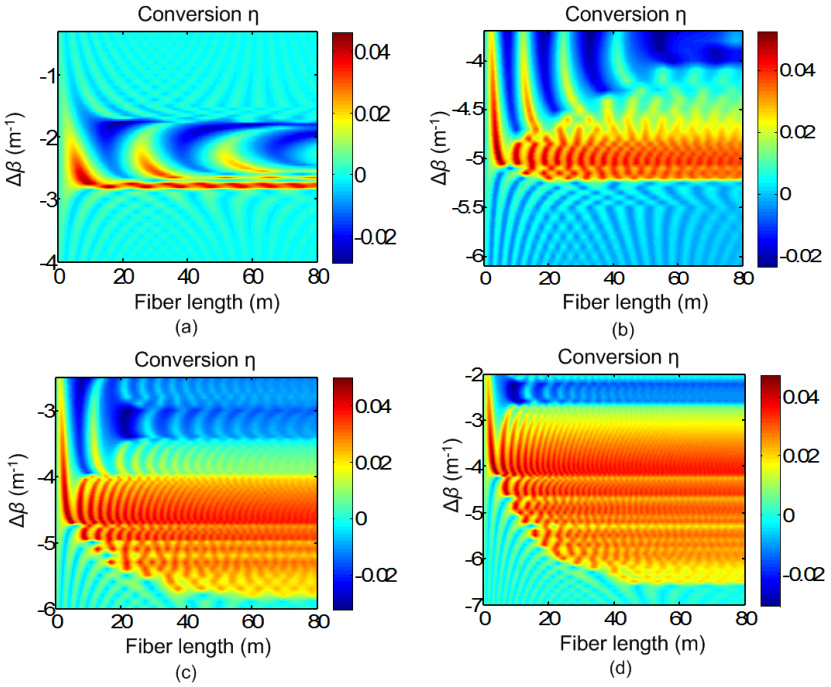

Fig. 8. Contour map of conversion efficiency in (a) 30 mol. %, (b) 60 mol. %, (c) 70 mol. %, and (d) 80 mol. % doping fiber plotted against propagation constant mismatch and fiber length

4. Conclusion

In summary, we have designed step-index HGDFs for phase-matched OTHG and analyzed the performances for different fibers. Parameters such as effective indices, core diameters, and overlap integrals for HGDFs with different doping concentrations were investigated. In specially designed HGDF with core GeO_2 doping levels of 90 mol. %, the pump loss is no longer a disadvantage and can be used to compensate the accumulated phase-mismatch dynamically along the fiber for efficient OTHG. According to our simulation, 31% conversion efficiency which is nearly 4 times higher than the equivalent lossless process is achievable over 34 m of fiber with a doping concentration of 90 mol. % in the core. The results demonstrate that HGDFs can potentially be applied for efficient OTHG which is significant in the area of triple photons generation and parametric amplification.

Acknowledgments

This work was supported by the Singapore A*STAR SERC Grant: “Advanced Optics in Engineering” Program (Grant No. 1223600001). G. Brambilla gratefully acknowledges the Royal Society (London) for his University Research Fellowship.

References

1. V. Grubsky and A. Savchenko, "Glass micro-fibers for efficient third harmonic generation," Opt. Express **13**(18), 6798–6806 (2005).
2. T. Lee, Y. Jung, C. A. Codemard, M. Ding, N. G. R. Broderick, and G. Brambilla, "Broadband third harmonic generation in tapered silica fibres," Opt. Express **20**(8), 8503–8511 (2012).
3. A. Coillet and P. Grelu, "Third-harmonic generation in optical microfibers: from silica experiments to highly nonlinear glass prospects," Opt. Commun. **285**(16), 3493–3497 (2012).
4. W. Gao, K. Ogawa, X. Xue, M. Liao, D. Deng, T. Cheng, T. Suzuki, and Y. Ohishi, "Third-harmonic generation in an elliptical-core ZBLAN fluoride fiber," Opt. Lett. **38**(14), 2566–2568 (2013).
5. F. Gravier and B. Boulanger, "Triple-photon generation: comparison between theory and experiment," J. Opt. Soc. Am. B **25**(1), 98–102 (2008).
6. M. Corona, K. Garay-Palmett, and A. B. U'Ren, "Third-order spontaneous parametric down-conversion in thin optical fibers as a photon-triplet source," Phys. Rev. A **84**(3), 033823 (2011).
7. S. Richard, K. Bencheikh, B. Boulanger, and J. A. Levenson, "Semiclassical model of triple photons generation in optical fibers," Opt. Lett. **36**(15), 3000–3002 (2011).
8. S. Afshar V, M. A. Lohe, T. Lee, T. M. Monro, and N. G. R. Broderick, "Efficient third and one-third harmonic generation in nonlinear waveguides," Opt. Lett. **38**(3), 329–331 (2013).
9. H. Takahashi and I. Sugimoto, "A germanium-oxide glass optical fiber prepared by a VAD method," J. Lightwave Technol. **2**(5), 613–616 (1984).
10. S. Sakaguchi and S. Todoroki, "Optical properties of GeO_2 glass and optical fibers," Appl. Opt. **36**(27), 6809–6814 (1997).
11. K. Kravtsov, Y. K. Huang, and P. R. Prucnal, "All-optical 160 Gbits/s time-domain demultiplexer based on the heavily GeO_2-doped silica-based nonlinear fiber," Opt. Lett. **34**(4), 491–493 (2009).
12. V. Kamynin, A. S. Kurkov, and V. M. Mashinsky, "Supercontinuum generation up to 2.7 μm in the germanate-glass-core and silica-glass-cladding fiber," Laser Phys. Lett. **9**(3), 219–222 (2012).
13. E. A. Anashkina, A. V. Andrianov, M. Yu. Koptev, V. M. Mashinsky, S. V. Muravyev, and A. V. Kim, "Generating tunable optical pulses over the ultrabroad range of 1.6-2.5 μm in GeO_2-doped silica fibers with an Er:fiber laser source," Opt. Express **20**(24), 27102–27107 (2012).
14. A. Efimov, A. J. Taylor, F. Omenetto, J. Knight, W. Wadsworth, and P. Russell, "Phase-matched third harmonic generation in microstructured fibers," Opt. Express **11**(20), 2567–2576 (2003).
15. K. Tarnowski, B. Kibler, C. Finot, and W. Urbanczyk, "Quasi-phase-matched third harmonic generation in optical fibers using refractive-index gratings," IEEE J. Quantum Electron. **47**(5), 622–629 (2011).
16. K. Bencheikh, S. Richard, G. Mélin, G. Krabshuis, F. Gooijer, and J. A. Levenson, "Phase-matched third-harmonic generation in highly germanium-doped fiber," Opt. Lett. **37**(3), 289–291 (2012).
17. J. W. Fleming, "Dispersion in GeO_2-SiO_2 glasses," Appl. Opt. **23**(24), 4486–4493 (1984).
18. A. Snyder and J. Love, Optical Waveguide Theory, 1st ed. (Springer, 1983).
19. A. Wada, S. Okude, T. Sakai, and R. Yamauchi, "GeO_2 concentration dependence of nonlinear refractive index coefficients of silica-based optical fibers," Electron. Commun. Jpn. Part Commun. **79**(11), 12–19 (1996).
20. E. M. Dianov and V. M. Mashinsky, "Germania-based core optical fibers," J. Lightwave Technol. **23**(11), 3500–3508 (2005).